The Self-Assembly of Redox Active Peptides: Synthesis and Electrochemical Capacitive Behavior

Julia P. Piccoli,[1] Adriano Santos,[2] Norival A. Santos-Filho,[1] Esteban N. Lorenzón,[1] Eduardo M. Cilli,[1] Paulo R. Bueno[2]

[1]*Department of Biochemistry and Technological Chemistry, , Institute of Chemistry, UNESP—Univ Estadual Paulista, São Paulo, Brazil*

[2]*Department of Physical Chemistry, Nanobionics Research Group, Institute of Chemistry, UNESP—Univ Estadual Paulista, São Paulo, Brazil*

Received 1 September 2015; revised 16 December 2015; accepted 14 January 2016
Published online 2 February 2016 in Wiley Online Library (wileyonlinelibrary.com). DOI 10.1002/bip.22815

ABSTRACT:

The present work reports on the synthesis of a redox-tagged peptide with self-assembling capability aiming applications in electrochemically active capacitive surfaces (associated with the presence of the redox centers) generally useful in electroanalytical applications. Peptide containing ferrocene (fc) molecular (redox) group (Ac-Cys-Ile-Ile-Lys(fc)-Ile-Ile-COOH) was thus synthesized by solid phase peptide synthesis (SPPS). To obtain the electrochemically active capacitive interface, the side chain of the cysteine was covalently bound to the gold electrode (sulfur group) and the side chain of Lys was used to attach the ferrocene in the peptide chain. After obtaining the purified redox-tagged peptide, the self-assembly and redox capability was characterized by cyclic voltammetry (CV) and electrochemical impedance-based capacitance spectroscopy techniques. The obtained results confirmed that the redox-tagged peptide was successfully attached by forming an electroactive self-assembled monolayer onto gold electrode. The design of redox active self-assembly ferrocene-tagged peptide is predictably useful in the development of biosensor devices precisely to detect, in a label-free platform, those biomarkers of clinical relevance. © 2016 Wiley Periodicals, Inc. Biopolymers (Pept Sci) 106: 357–367, 2016.

Keywords: self-assembly; redox probe peptide; electroactive peptide; electrochemical characterization; redox peptide monolayers

Correspondence to: Eduardo M. Cilli, Department of Biochemistry and Technological Chemistry, Institute of Chemistry, UNESP—Univ Estadual Paulista, São Paulo, Brazil; e-mail: cilli@iq.unesp.br and Paulo R. Bueno, Department of Physical Chemistry, Nanobionics Research Group, Institute of Chemistry, UNESP—Univ Estadual Paulista, São Paulo, Brazil; e-mail: prbueno@iq.unesp.br

Contract grant sponsor: São Paulo Research Foundation
Contract grant numbers: FAPESP2012-22820-7; FAPESP2015-02343-8
Contract grant sponsor: Brazilian National Council for Scientific and Technological Development (CNPq) Grants

This article was originally published online as an accepted preprint. The "Published Online" date corresponds to the preprint version. You can request a copy of any preprints from the past two calendar years by emailing the Biopolymers editorial office at biopolymers@wiley.com.

INTRODUCTION

In last decades there has been a focused research in metal surfaces modification by forming ordered and structurally controllable molecular layer architecture within the context of obtaining stable and functional molecular junctions where the well-known self-assembled monolayers (SAMs) are the ultimate and the largest studied man-made molecular interfaces,[1] comprising different applications going from biosensors[2–5] to dye-sensitized solar cells.[6,7] Furthermore, many natural processes such as protein folding, hybridization of DNA and cell membranes formation involve chemical concepts within the scope of self-assembling and/or self-organization[8,9] of molecular and supramolecular structures. For instance, natural processes

governed either by inter and intra molecular forces such as those including hydrogen bonding, electrostatic interactions, hydrophobic interactions, and Van der Waals forces[9,10] are within these broad scope. Accordingly self-assembled monolayers formation over conductive interfaces is one of the easiest methods to obtain ordered man-made monolayers, through chemisorption, for example, between them and a metal surface, stimulating the preparation of man-engineered thermodynamically stable monolayers.[11]

SAMs are nowadays routinely used in many areas such as surface wetting, non-fouling surface structures, electrochemistry, surface passivation, protein binding, DNA assembly, corrosion protection, biological arrays, cell interactions, and molecular electronics[12–16] to mention but a few. Among the latter mentioned range of applications, one interesting, which will be the focus of the present work, is the electrochemistry of engineered multi-function electroactive monolayer. In this way many authors explore the thermodynamic basics of SAM formation and infer information about structural conformation through electrochemistry characterization.[17] This means that the knowledge of SAMs structural characteristics constitutes an important tool mainly related to the control and development of electroanalytical applications. For instance, SAMs are generally used to report selective analytes of interest by applying suitable monolayers constructed over conductive electrodes,[15] offering controlled properties of the surface and distinctive reactive backgrounds and possibilities by using redox molecules as probe in the screened electrolyte environment.[18] Accordingly SAMs are nowadays routinely applied in merging biosensor technology and nanotechnology,[9,17] truly opening doors toward directive surface engineering with a multitude of applications ranging from materials science to analytical chemistry.[19,20] Within the electron analytical context, self-assembled monolayer allows the suitable control of the electrode transducer signal,[21] for instance. The simplest electroanalytical system are based on monolayers that provide selective access to the electrode's signal by means of a specific recognition fragment.[17] On the latter context, the main advantage is that monolayers offer spatial control such as an appropriate orientation of the receptor to detect target, enhancing the specificity and preventing interferences.[22]

It was in 1980's that it was discovered that alkanethiols spontaneously assembled on metals surfaces[23] and since then metallic surfaces have being the preferable functionalized surfaces. These interfaces are designed accordingly to applications but mainly it can be observed those based on aromatic molecules, hydrogen-bonded molecules with functional groups like thiols, amines, sulphides, selenides among others that offer enhanced stability to the desirable molecular assembled layers.[24] Newly uses are yet possible such as those based on SAMs comprising alkanethiols within a probe redox as the electrochemical active group whose electron activity can be applied as transducer signal. This type of electroactive surface and structure has been shown to be of major importance in achieving reliable electrochemical capacitive biosensors as we reported recently.[25] Latter application comprises development of medical diagnostics devices.[26] Significant is the fact that electroactive monolayers are valuable for the immobilization of antibodies, proteins, biological molecules, enzymes, aptamers, and others receptors on metal surfaces underpinning a variety of electrochemistry applications in a multiplexing manner.[27] In general, electrochemistry-based sensors using SAMs as the main building blocks have been employed for example, to monitoring pH, inorganic species, organic molecules and important biomolecules, the latter by using the chemical and biological recognition approach.[28,29] Yet biocomposites synthesis has been reported based on SAM templates.[30] For example, self-assembly of peptides monolayers on gold surface demonstrated good characteristics as an alternative to those comprising traditional monolayers.[26] In summary, self-assembly molecular layers are very suitable and desirable in different applications and peptides-based molecular function constitutes useful and versatile alternative to be exploited in those kinds of applications, as we will demonstrate below.

The fact that the peptide molecules can be built by using twenty amino acids as building blocks has turn the development of "Solid Phase Peptide Synthesis" (SPPS)[31] into a reality. This is an effective methodology to synthesize different functional molecules, offering an easy preparation and purification methodology and thus providing the ability to design reliable molecular functional structures over electrodes within a multitude of structural and physical-chemistry properties.[17] Additionally the simple and versatile characteristic involving SPPS allows add redox probes into the amino-acid chains.[26] By designing peptides with self-assembling characteristics it is possible to achieve competitive and yet superior versatility, for instance, non-fouling surfaces. For instance, peptides self-assembled monolayers are fabricated in a way that surface properties are remarkably adapted to the desirable applications.[15] Regarding electrochemistry applications, electrochemical techniques such as cyclic voltammetry and impedance/capacitance measurements are useful in monitoring molecular layer structural characteristics and electrical (conductive or dielectric) properties.[32] For instance, we have recently demonstrated that the self-assembling characteristics of peptides containing a probe redox molecule, in particular ferrocene, deposited over metallic gold surface are interesting in developing alternative capacitive biosensor.[33] The sensoring capability is based on obtaining the electrochemical capacitive signal of the synthesized redox-tagged peptide by using Electrochemical

Capacitance Spectroscopy (ECS).[25,33] Some authors used peptides labeled with a redox probe, most frequently ferrocene, to detect various biological proteins as well as enzymatic activities using traditional electroanalytical approaches,[34,35] but rarely the sensoring signal is based on the electrochemistry capacitance.

In biosensor applications, peptides monolayers have important advantage over traditional monolayers once peptide monolayers are able to reduce the non-specific interaction (potential perturbative signal) caused by the huge amount of non-specific protein intrinsically contained in complex biological samples such as patient blood. As a result, an increase in selectivity compared with typical low fouling surfaces like PEG[15] is possible to be achieved. Highly important is that peptide functions are not only useful on the formation of monolayers but additionally can act, at the same time, as receptive layer being very desirable in biosensors applications.[36] Because peptide monolayers constitute an all-in-one alternative, they comprise sequences able to contain assembling capability (surface anchoring functions to functionalize the electrode) and biomolecular recognition within an ultra-low fouling platform besides containing redox activity by comprising additional redox sites.[37]

Within this context of multi-functionality it is clear that electrochemistry biosensor devices demand applications of engineered peptide layers. Indeed, it has been shown that peptide-based assays have additional comparative advantages such as high speed and sensitivity over those more traditional assays[32] by either reducing the chemical steps needed during surface's fabrication and by lowering costs[38,39] during fabrication of the devices. As a final examples, peptides which cleavage enzymes can be used to detect important enzymes like PSA, one of the main markers of prostate cancer,[40,41] without needs of antibodies or receptive biomolecule over the electrodes surface. It has been shown that some protein kinases can been linked to many forms of cancer, recently, Wang and coworkers used a peptide and a modified FC-ATP (adenosine triphosphate) to detect kinase-catalyzes phosphorylation.[42]

We report herein on the synthesis, by solid phase, of an electrochemical active peptide with self-assembling capability that can be used as redox-tagged peptide in electrochemical capacitive biosensoring surface.[26,43] Basically the peptide-based self-assembly monolayer is comprised of a ferrocene-tagged group whose electrochemistry activity was characterized by traditional and by a newer capacitive-based methods.

MATERIALS AND METHODS

Chemicals

Solutions were prepared with Milli-Q® water (Millipore Reagent Water System, USA) with 18.2 MΩ cm at 25°C. All the Fmoc (9-fluorenylmethyloxycarbonyl) amino acids and resins were purchased from Sigma Aldrich Co. (USA) and AAPPTEC (USA). Solvents and reagents for peptide synthesis were obtained from Sigma Aldrich Co. (USA) and Fluka (USA). DCM (dichloromethane) and DMF (dimethylformamide) were purchased from Hexis Cientifica and VETEC (Brazil). 3-Ferrocenylpropionic anhydride was purchased from Sigma Aldrich Co (USA). Acetonitrile (ACN) was purchased from Panreac and tetrabutylammonium perchlorate ($TBAClO_4$) was purchased from Sigma-Aldrich (USA).

Peptide Synthesis

The peptide Ac-Ile-Ile-Lys-Ile-Ile-COOH was automated produced by solid phase peptide synthesis (SPPS) using a PS3 synthesizer (Protein Technologies) through Fmoc protocols on Fmoc-Ile-Wang Resin (0.67 mmol g^{-1}). Methyltrityl group (Mtt) protected the side chain of Lys residue. Coupling was performed at twofold excess over the amino component in the resin, using N,N,N′,N′-Tetramethyl-O-(1H-benzotriazol-1-yl) uroniumhexafluorophosphate (HBTU)/N-methylmorpholine (NMM). The Fmoc group was deprotected by 20% N-methyl-piperidine/dimethylformamide (DMF). After the synthesis, the side chain of Lys (Mtt) was deprotected by 1% trifluoroacetic acid (TFA) in dichloromethane (DCM) and the success of the coupling was monitored by ninhydrin reaction. When the ε amino group (primary amine in the Lys side chain) of Lys was free, 3-ferrocenylpropionic anhydride was attached by incubation in presence of DCM (dichloromethane) and DMF (dimethylformamide) for 24 h, resulting in the peptide Ac-Ile-Ile-Lys(fc)-Ile-Ile-COOH. Cleavage of the Wang resin and removal of the side chain protecting groups were performed with 94% TFA, 2.5% 1,2-ethanedithiol (EDT), 2.5% H_2O, 1% triisopropylsilane (TIS) for 2 h. After this, the peptide was precipitated with ethyl ether anhydrous, separated from soluble non peptide material by centrifugation, extracted in a mixture of 0.045% (v/v) TFA/H_2O and 0.036% (v/v) TFA/ACN and lyophilized. The crude product was purified by HPLC system on a Beckman System Gold using a semi-preparative reverse phase Phenomenex Jupiter C18 column (250 x 10 mm), packed with spherical 5 μm particle and 300 Å pore size. A linear gradient elution was employed from 30 to 80% of solvent B (0.036% (v/v) TFA/ACN) for 105 minutes. The flow rate was 5 mL/min at room temperature and the injection volume was 5 mL, UV detection was carried out at 220 nm. The purity of peptide was analyzed using an analytical Shimadzu system with a reverse phase Phenomenex Jupiter C18 column (150 x 4.6 mm), packed with spherical 5 μm particle and 300 Å pore size, linear gradient of 5 to 95% of solvent B for 30 min, flow rate of 1.0 mL min^{-1} and UV detection at 220 nm. The identity of the peptide was analyzed in an ion-trap Mass Spectrometer using a Brucker system in positive mode.

Electrode Surface Preparation

Mechanical polishing using aluminum oxide pads with decreasing particle sizes (1 μm, 0.3 μm, and 0.05 μm) prepared the gold surface. Sonication in water was performed between polishing steps to remove adhered particles. The electrode surfaces were then electrochemically cleaned in deaerated NaOH 0.5 M (−1.5 V and −0.5 V at a scan rate of 50 mV s^{-1}) and subsequently in 0.5 M H_2SO_4 (−0.2 V and 1.5 V at a scan rate of 100 mV s^{-1}) until stabilization of the gold reduction peak in CV was attained (approximately 50 cycles). Following electrochemical polishing, electroactive areas were evaluated by

mathematical integration of the cathodic peak with the potential from gold electropolishing voltammograms and converted to the real surface area, using a conversion factor of 400 μC cm^{-2} [44] The roughness factor was controlled by maintaining it between 1.2 and 1.5 in all measurements.

Surface Architecture and Electrochemical Measurements

A cleaned Au electrode (as detailed in the previous section) was immersed for 16 h at 25°C in a solution containing 1.8 mmol L^{-1} of the electroactive peptide in water/acetonitrile(50:50) for the formation of the self-assembled monolayer. An AUTOLAB potentiostat (PGSTAT30) with a FRA module controlled using the NOVA software was used for all electrochemical measurements. A three-electrode setup consisting of a gold working electrode (2.0 mm diameter) from METROHM, a platinum mesh counter electrode, and an Ag|AgCl (saturated KCl) reference electrode were used for the measurements.

Electrochemical characterization was conducted using a supporting electrolyte of 20 mM $TBAClO_4$ dissolved in acetonitrile and water (20:80, v/v) without a redox probe. Cyclic voltammetry (CV) was performed at a scan rate of 100 mV s^{-1} between 0.0 V and 0.7 V relative to Ag|AgCl. Electrochemical Impedance Spectroscopy (ESI) measurements were conducted at the half-wave potential ($E_{1/2} = 0.37$ V) and non-Faradaic (redox out) region (0.10 V), at a frequency ranging from 100 kHz to 10 mHz, with a peak-to-peak amplitude of 10 mV. Measurements were verified for compliance with Kramers–Kroning linear systems theory using the NOVA software. Electrochemical Capacitance Spectroscopy (ECS) analysis was performed by determining the capacitance, using the relationship $C^*(\omega)=1/i\omega Z^*(\omega)$, where ω is the angular frequency and i is the complex number $=\sqrt{-1}$.[33] In processing $Z^*(\omega)$, it is possible to obtain both the imaginary $C''=\varphi\ Z'$ and real $C'=\varphi\ Z''$ portions of capacitance, noting that $\varphi=1/(\omega|Z|^2)$, where $|Z|$ is the modulus of impedance. The peptide surface coverage (Γ, mol cm^{-2}) was calculated using the equation $\Gamma=4C_r k_B T/eF$, providing an occupation at the half-wave potential where $f=1/2$ (where the redox capacitance, C_r, maximizes), [see Eq. (1) below for more details], where k_B is the Boltzmann constant, T is the absolute temperature (293 K), and e is the elementary charge.[26] To compare the Γ results obtained using the redox capacitance approach, the surface coverage was estimated using an expression derived from classical voltammetry $\Gamma=Q/n_eFA$, where n_e is the number of electrons in the electrochemical reaction ($n_e = 1$, since $Fc^+ + e^- \leftrightarrows Fc$) and Q is the charge obtained by the integration peak of the reduction/oxidation process in the CV, discounting the capacitive contribution. Noting that $Q=(1/\nu)\int idV$, where i is the current, ν is the scan rate, and A is the electrode electroactive area (cm^2), determined as previously described.[45]

RESULTS AND DISCUSSION

Peptide Synthesis

To prepare the peptide containing ferrocene molecular group, the peptide Ac-Cys-Ile-Ile-Lys-Ile-Ile-COOH was synthesized by Fmoc-strategy, using Wang-Ile resin and Mtt as side chain protective group of Lys. The Wang resin was chosen to obtain a peptide with free carboxyl in the C-terminal group. This free carboxyl group is important for further coupling of an antibody, enabling the use of the peptide in molecular recognition applications such as by forming functionalized surface for biosensor applications[26] when coupled to a metallic plate. The amino acid Isoleucine was chosen due to the hydrophobicity and volume of side chain,[46] resulting in the presence of hydrophobic and intramolecular hydrogen bonding in the peptide molecules.[47] The volume of the branched increased in the order alkanethiol < Ala < Ile.

Afterward the Fmoc-Cys(tBu), coupling and deprotecting, the N-terminal of the peptide was acetylated to avoid further possibilities of reactions, mainly the reaction with C-terminal group. With the peptide still in the resin, the protecting group Mtt was selectively removed by using DCM containing 1% of TFA (twice by 30 min). Subsequently the resin was submitted to ninhydrin test, showing a positive result, regarding free amino groups. To make the conjugate, one equivalent of 3-ferrocenylpropionic anhydride and one equivalent of resin-peptide was placed in presence of DCM and DMF during 24 h, after a positive ninhydrin test, other solvents were evaluated: DCM containing 50% of NMP (N-Methyl-2-pyrrolidone) during 24 h (not effective), and then, DCM containing 10% of HFIP (1,1,1,3,3,3-Hexafluoro-2-propanol) during 24 h. The 3-ferrocenylpropionic anhydride carboxyl group is reactive, attaching to ε amino group Lys and forming an amide bond,[48] resulting in the following Ac-Cys-Ile-Ile-Lys(fc)-Ile-Ile-COOH peptide chain.

Different cleavages solutions were tested to obtain an optimized protocol to synthesize ferrocene-peptide conjugate. Solutions containing 94% TFA, 2.5% H_2O, 2.5% EDT and 1% TIS (1); 82.5% TFA, 5% TIS, 5% H_2O, 5% phenol and 2.5% EDT (2); 95% TFA and 5% H_2O (3); 95% TFA, 2.5% TIS and 2.5% H_2O (4) were used. The cleavage was successful when the solution (1) was used and the synthesis of the ferrocene-peptide was performed in the resin at the side chain of Lys, with the Fmoc protocol, as demonstrated in the crude peptide chromatogram in Fig. 1a.

Furthermore, as can be seen in Fig. 1a, the peak associated with ferrocene-free peptide is still present after the synthesis. Allowing two different possibilities: selective removal of the Mtt group was not efficient enough to prevent the attachment of ferrocene molecule to the ε amino group of Lys, or, the reaction of ferrocene molecule to the amino group was not completed. In both situations we have a combination of two compounds: Ac-Cys-Ile-Ile-Lys-Ile-Ile-COOH and Ac-Cys-Ile-Ile-Lys(fc)-Ile-Ile-COOH, as shown in the chromatogram in Fig. 1a. The peaks around 22.8 and 28.8 minutes in the Fig. 1a are assigned to a contaminant produced during the synthesis. The ferrocene-free peptide exhibits a retention time of 16.0 minutes

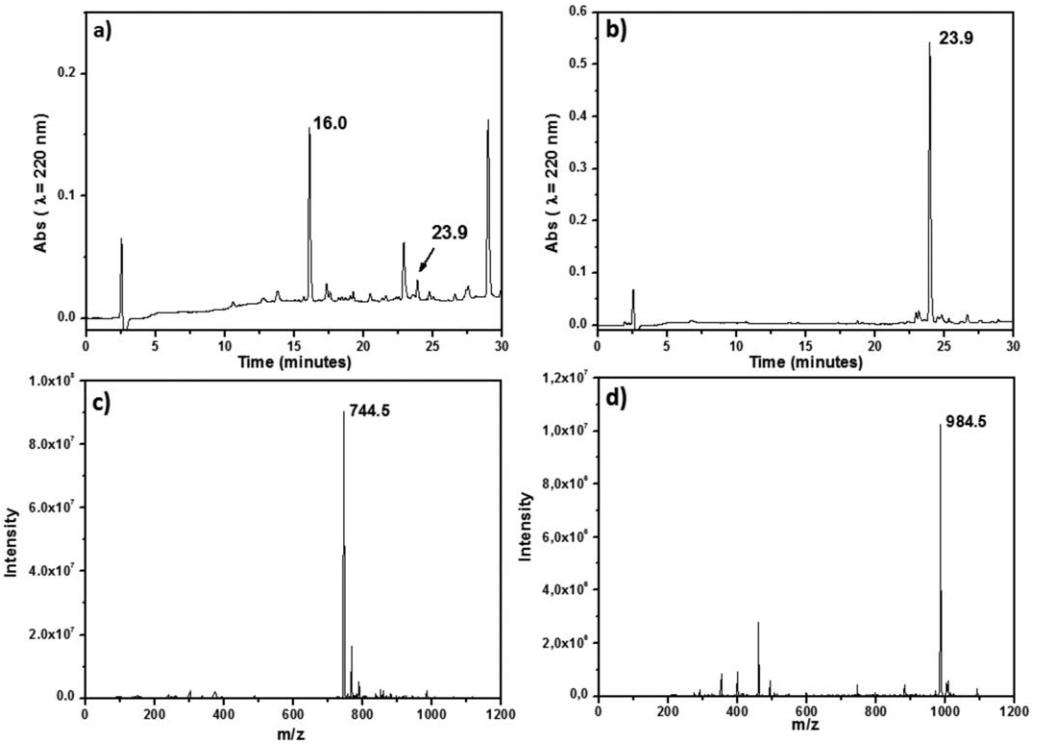

FIGURE 1 (a) Chromatogram of the crude ferrocene-tagged conjugate peptide [analytical reverse phase Phenomenex Jupiter C18 column (150 x 4.6 mm), packed with spherical 5 µm particle and 300 Å pore size, using a linear gradient of 5–95% (v/v) of solvent B for 30 min, at a flow rate of 1.0 mL/min and UV detection at 220 nm]. (b) Chromatogram of the purified ferrocene-peptide conjugate, i.e. purity > 95% [analytical reverse phase Phenomenex Jupiter C18 column (150 x 4.6 mm), packed with spherical 5 µm particle and 300 Å pore size, using a linear gradient of 5–95% (v/v) of solvent B for 30 min, at a flow rate of 1.0 mL/min and UV detection at 220 nm]. (c) Mass spectrum of the ferrocene-free peptide: 744.5 g moL $^{-1}$ – relative peak of 16.0 min in (a). (d) Mass spectrum of the redox-tagged conjugate peptide: 984.5 g moL $^{-1}$ – relative peak of 23.9 min in (a).

meanwhile the ferrocene containing peptide has a retention time of 23.9 minutes. The mass spectrum of both ferrocene-free and peptide containing ferrocene are shown in Figs. 1c and 1d.

The obtained difference in the retention times (R_t) enable the purification of the ferrocene redox-tagged peptide and so that it was possible to obtain a pure ferrocene-peptide as evidenced in Fig. 1b (> 95%). The characteristic of the ferrocene-free and redox-tagged peptide are summarized in the Table I.

Electrochemical Characterization

After obtaining the purified redox-tagged peptide the appropriate electrochemical characterization was performed by self-assembling the peptide into gold electrodes. The capability for self-assembly of the synthesized redox-tagged peptide is expected to occur via thiol group present in the Cys residue. The electrochemical behavior was thus evaluated by using CV and EIS by comparing the obtained results with those observed for a bare/cleaned gold surface (i.e., the electrode in the absence of peptide). As shown in Fig. 2 the oxidation and reduction peaks associated with the ferrocene/ferrocenium (Fc/Fc^+) redox coupling activity were clearly observed in the CV plots. The formal potential was found to be approximately 0.37 V relative to the Ag|AgCl reference. The difference between the oxidation and reduction potential peaks is nearly 18 mV and the ratio between j_{pa} to j_{pc} (i.e., the ratio between

Table I Characteristics of the Ferrocene-free and Ferrocene-tagged Peptides

Peptide	Calculated mass (g moL^{-1})	Measured mass (g moL^{-1})	R_t (minutes)
Ac-Cys-Ile-Ile-Lys-Ile-Ile-COOH	744.0	744.5	16.0
Ac-Cys-Ile-Ile-Lys(fc)-Ile-Ile-COOH	984.5	984.5	23.9

R_t comprises for retention time.

the anodic and cathodic current density peaks) is about unit. From both results, it is clear that the redox-tagged peptide was successfully attached onto gold's electrode surface presenting a characteristic (or typical) redox reversible process.

It has been discussed in literature that the fingerprint of redox tagged peptide monolayer could be evaluated by the peaks and shapes of the CV[49] pattern. It is said that for an ideal free-of-defects redox SAM, a condition without dispersive electron transfer rate constant k_r,[49,50] the full width at half of the peak maximum height (FWHM) should present, for a single electron transfer process, a value corresponding to $FWHM = 90.6\ mV$ [49,50] in the CV. This analysis is based on those behavior expected for redox free species in solution phase where classical analysis applies (since ions are treated as Boltzmann particles, following a Boltzmann distribution of states), i.e. the electron transfer are believed to follow a Nernst distribution of redox potentials. Nonetheless, for electroactive monolayers chemically attached over electrodes quite frequently deviations of Nernst distribution of redox potentials is observed because essentially the redox particles now are chemically coupled to the metallic states where the electron is a Fermion particle, following a Fermi-Dirac distribution with energy instead of a Boltzmann distribution. Because of latter, the redox monolayer is mesoscopic in essence and their dispersive potential behavior affects electron transfer as discussed recently by Bueno *et al.*[51] According to quantum mechanics statistics the monolayers behaves as "molecular solids" with redox species contributing for the existence an electrochemical density of states following a Gaussian pattern that spreads energetically depending on the energetic structural rearrangement of the molecular layers as an ensemble of redox states following the Fermi occupation modulated by the electrode. In this picture deviations from the pure Nernst distribution of redox states are obviously dependent on the dielectric environment and vary reversibly for the same monolayer at different dielectric environment. Deviations on redox potentials are, therefore, not particularly associated with molecular layer preparation or synthesis but depend on how the electronic quantum states on the molecular layer is occupied energetically, spreading with dielectric environment. This is expected to vary differently for the same molecular layer depending on the external environment and electrochemical potential.

For instance, by considering a single redox state chemically coupled with metallic electrode, the capacitance is given by

$$C_r(\bar{\mu}) = \frac{e^2\Gamma}{k_B T} f(1-f) \tag{1}$$

where C_r is the redox capacitance, k_B is the Boltzmann constant, T is the absolute temperature (293 K), and e is the elementary charge. Note that f is the Fermi-Dirac distribution $f = \{1+\exp[(\bar{\mu}-E_r)/k_B T]\}^{-1}$, where k_B is the Boltzmann constant. Eq. (1), for $f = 1/2$ (that is the for capacitance values obtained at half-wave potential). Based in Eq. (1) the molecular redox coverage can be estimated as $\Gamma = 4C_r k_B T/eF$ (as previously indicated in the experimental section). Hypothetically at zero-temperature limit Eq. (1) turns into $C_r(\bar{\mu}) = e^2 g_r(\bar{\mu}) = e^2 dN_r/d\bar{\mu}$.

$$C_r(\bar{\mu}) = e^2 \int_{-\infty}^{\infty} g_r(\bar{\mu}) \frac{df}{d\bar{\mu}} d\bar{\mu} = \frac{e^2}{k_B T} \int_{-\infty}^{\infty} g_r(\bar{\mu}) f(1-f) d\bar{\mu} \tag{2}$$

where $g_r(\mu) = dN_r/d\bar{\mu}$ is the redox density of states that can be realistically written as

$$g_r(\bar{\mu}) = \frac{dN_r}{d\bar{\mu}} = \frac{1}{\sigma_g\sqrt{2\pi}} \exp\left[-\frac{(\bar{\mu}-E_r)^2}{2{\sigma_g}^2}\right] \tag{3}$$

i.e., a Gaussian function with the normal distribution centred at E_r (the energy of the redox states) and with a σ_g standard deviation (${\sigma_g}^2$ variance). Any change in redox site occupancy is thus integrated into $g_r(\bar{\mu})$ and experimentally reported through C_r.

The N_r (the density of redox states) is then occupied according to electrochemical chemical potential of the electrons in the electrode following the Gaussian DOS shape where k_B is the Boltzmann constant and T the absolute temperature. It corresponds (or the number of electronic states in the molecular layer) exactly to $N_r = \Gamma$ assuming the existence of electrons as particles (not waves) that occupies a single ferrocene molecule in the molecular layer, without any quantum mechanics/mesoscopic effects associated with the redox peptide molecular layer. Note also that $\bar{\mu}$ (the electrochemical potential of electrons in the electrode) is related to the Gibbs free energy of a single electron transfer step according to $\Delta G_r = E_r - \bar{\mu}$, where the electrical work defined by edV translates into associated with change in free energy and ultimately stored chemical energy, i.e. $d\bar{\mu}$.

Following this ideas it can be observed that from the CV results shown in Figure 2a, both cathodic and anodic peaks exhibit larger value of FWHM ($\sim 100\ mV$) than those expected SAM Nernst idealistic behavior. Accordingly both values obtained for capacitance by CV ($\sim 18\ \mu F\ cm^{-2}$) and capacitance spectroscopy (Figure 4*c* at redox out potential, $\sim 14\ \mu F\ cm^{-2}$) suggest that mesoscopic effects are present in the peptide redox SAM. The similarity between the capacitance values obtained by capacitance spectroscopy and CV is expected since we have shown in previous works that the redox capacitance of a redox layer is associated with CV currents and scan rate by $C_r = i/s$, where i is the current obtained in the CV

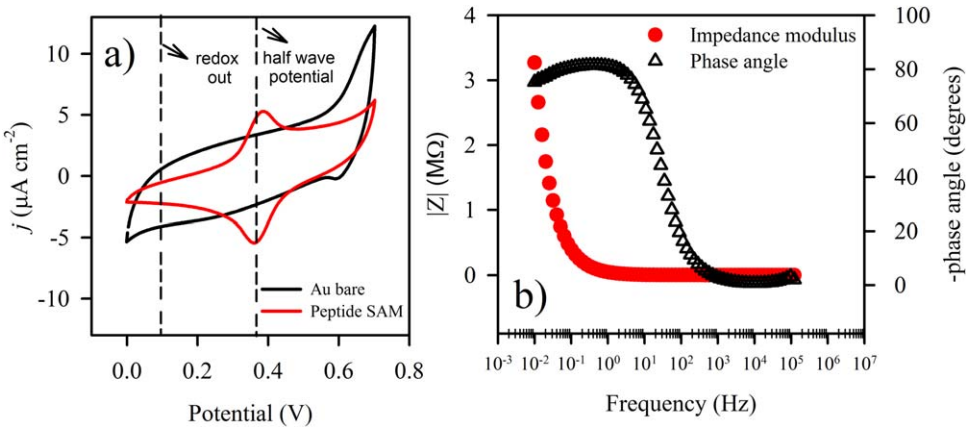

FIGURE 2 (a) Cyclic voltammetry for ferrocene modified peptide SAM. The *half wave* (or formal) potential (0.37 V) and *redox out* (0.1 V) lines denote regions where ECS was performed, as described in experimental section of the main text. The presence of anodic and cathodic peaks in the peptide SAM (red line), which are absent in bare gold CV (black line) are the characteristic evidence for successful immobilization of the redox-tagged peptide self-assembled over gold electrode. (b) Bode modulus plot (red circles) and Bode phase plot (black triangles) acquired at the half wave (or formal) potential. Note also that the modulus of impedance increase in regions about 10 Hz. A capacitive response is observed at low frequencies (below 10 Hz) meanwhile a pure resistance response is obtained at high frequencies (above 1 kHz). CV measurements were performed at a scan rate of 100 mV s^{-1} from 0.0 V to 0.7 V (V x Ag| AgCl), using a 20 mM $TBAClO_4$ solution as the supporting electrolyte and EIE were performed using 20 mM $TBAClO_4$ at 0.37 V.

and *s* is the potential scan rate. The capacitance obtained by capacitance spectroscopy is, nonetheless, more precise since it corrects non-faradaic contributions existing in the current response of CV methods, see also legend of Figure 3 and associated discussion for more details.

Following above theoretical background, EIS measurements were conducted at the formal potential (0.37 V) aiming to establish the characteristic electrochemical pattern of the redox-tagged peptide SAM. An increase in impedance was seen in frequencies about 10 Hz (Fig. 2b). The phase angle was also

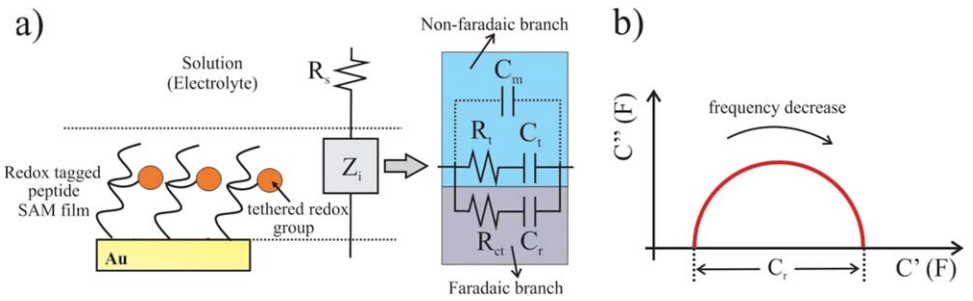

FIGURE 3 (a) Schematic representation of a redox-tagged peptide film comprising the interfacial impedance ($\boldsymbol{Z_i}$) and the solution resistance ($\boldsymbol{R_s}$). The equivalent circuit capable of modelling electrochemical redox capacitive interfaces is comprised of two series capacitances: a monolayer ($\boldsymbol{C_m}$) and a double-layer ($\boldsymbol{C_{dl}}$), where $\boldsymbol{C_{dl} \gg C_m}$. Since $\boldsymbol{C_m}$ dominates in analyses it is solely represented in the equivalent circuit model [33,53,56]. The dipolar response of the monolayer is represented by resistive ($\boldsymbol{R_t}$) and capacitive terms ($\boldsymbol{C_t}$). Note that $\boldsymbol{C_m \ll C_t}$, consequently $\boldsymbol{R_t}$ and $\boldsymbol{C_t}$ control the monolayer dielectric (ionic) response. In contrast, $\boldsymbol{R_{ct}}$ (charge transfer resistance) and $\boldsymbol{C_r}$ (redox capacitance) control the faradaic response. (b) $\boldsymbol{C_r}$ can be detected as a consequence of the electrochemical energy storage capability of the SAM over gold electrode interface. Note that $\boldsymbol{C_r}$ is easily determined from the diameter of the semicircle of the capacitance Nyquist plot [57] shown in (b). Details about the equivalent circuit representation of the surface process as illustrated herein can be found in references 26,27.

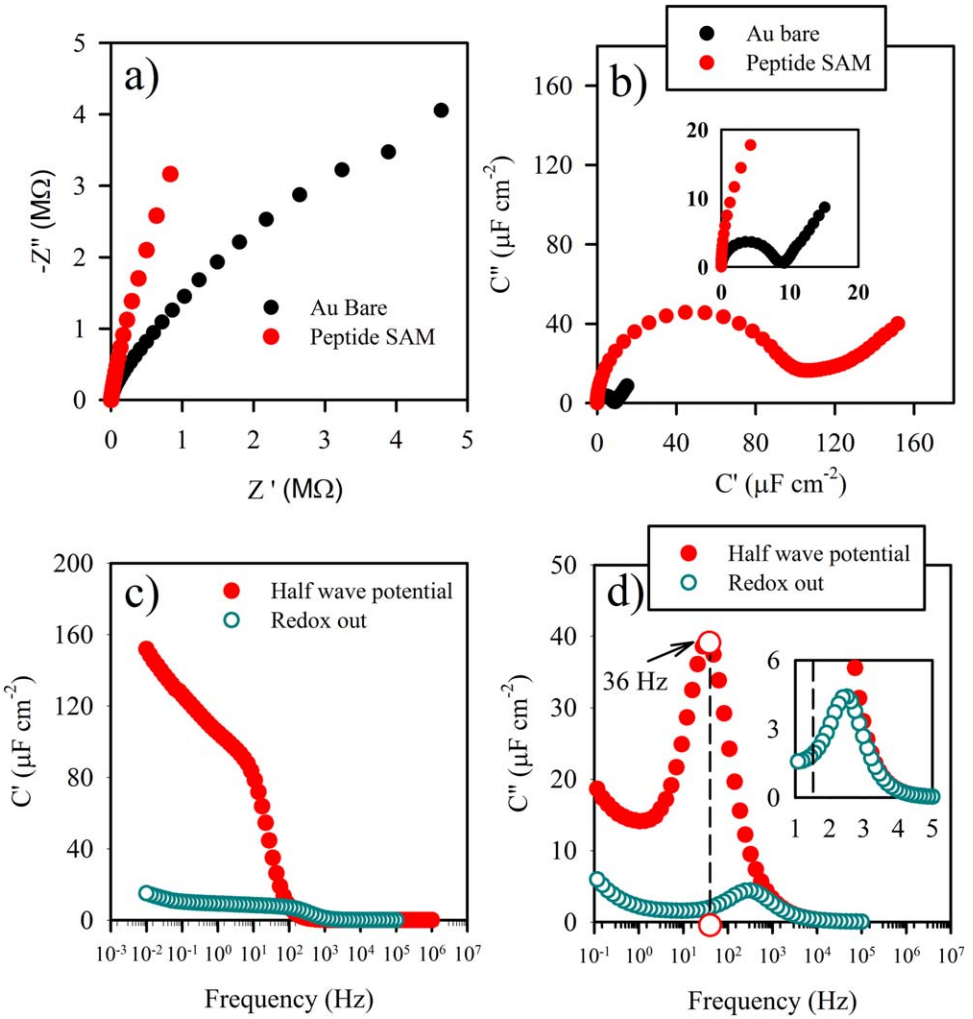

FIGURE 4 Impedance (a) and capacitance (b) Nyquist plots for redox tagged peptide immobilized above gold surface. From (b), it is clear an increase in capacitance values from ~10 μF cm^{-2} obtained to bare gold electrode (related to double layer capacitance) to ~105 μF cm^{-2} (redox tagged peptide SAM). (c) Real part of the capacitance of the ferrocene-tagged peptide film complex at electrode potentials corresponding to *redox in* (half wave potential) and *redox out* (0.1 V × AgIAgCl) potentials. Both contributions were modulated using the circuit shown in Fig. 3 (d) The same as (c), but representing the imaginary part of the complex capacitance response. The inset in (d) shows a magnified capacitance response in the *redox out* potential for the imaginary part of complex capacitance. Note that in the *redox out* potential, shown in (c) and (d), no significant contributions to the real and imaginary capacitance were observed, clearly demonstrating the redox activity of the ferrocene modified peptide which dominates over electrostatic and ionic polarization signals.

recorded for all frequency range and allows establish the resistive and capacitive contributions from measurements of the impedance magnitude. As well known, a zero phase angle corresponds to a current passing through a resistor (i.e. the voltage perturbation and the response current are in phase). On the other hand, a shift of −90° between the current and voltage is typical of a capacitance behavior. From the Bode plot (Fig. 2b), the resistance contribution occurs mainly at high frequencies (zero phase angle), while the capacitive contribution in the impedance spectrum is observed mostly at low frequencies.

The impedance behavior of a redox-active SAMs can be modeled using an appropriate equivalent circuit (Figure 3a). A detailed discussion about the equivalent circuit[33,52,53] and about redox capacitance and associated methodology can be found in references[26,27,33,53]. From this methodology (summarized in the Figure 3), it is possible to extract the capacitance and other resistive elements. Briefly, the circuit describes the

charging capability of this redox tethered interface, a physical chemistry feature obtained from the redox capacitance term C_r [26,27,54,55]. This charging fingerprint can be easily obtained converting the impedance spectra to capacitance (Figure 4). From these results, it is clearly observed an increase in capacitance (obtained approximately from the diameter of the semicircle as shown in capacitive Nyquist Plot of Figure 4b) from bare gold to redox peptide SAM. The redox capacitance change from $\sim$10 μF cm^{-2} (mainly due to the double layer capacitance) to$\sim$105 μF cm^{-2}, the latter provided by the redox (centers) activity of the molecular peptide layer, being higher than double layer (or equivalent non-faradaic) contributions.

The results of Figure 4 corroborate with voltammetry data (Figure 2a) and reinforce the well-defined formation of the SAM over the gold electrode[25]. In addition, Figures 4c and 4d show the Bode capacitive diagrams of redox in (red circles) and redox out potentials (blue open circles). Specifically note that in Figure 4d the redox relaxation peak (about 36 Hz), associated with the electron transfer rate, is absent for measurement taken at a *redox out* potential (as indicated in Figure 2a). This is due to the fact that the response is obtained at a potential outside of the redox activity of the electrode (named redox out) where faradaic response is absent so that evidencing a clear contribution (or its absence) of the redox active groups incorporated in the ferrocene-tagged peptide layer on the capacitive response observed comparatively when measured at potentials out or inside electrochemical activity. Furthermore, both real and imaginary capacitive components are highly responsive at the formal (redox inside) potential and practically unresponsive at redox out potential, once more clearly corroborating the redox activity of the ferrocene modified peptide layer which dominates the response over electrostatic and ionic polarization signals[26,33,53].

As demonstrated previously[33], the characteristic frequency in faradaic process of a redox tethered specie in an electroactive layer is related to the electron transfer rate constant (k_r), which can be extracted analyzing Bode plot (Figure 4d)[33,58–60]. This important observation discussed and exemplified in the literature demonstrated the versatile feature of capacitance spectroscopy in easily elucidating electrochemical features (equivalently but more precise than traditional methods, such as cyclic voltammetry) of this redox tethered monolayers, especially kinetics process, when certain experimental conditions are properly observed (i.e. measurements carried out at half-wave potential where the electronic redox sites/electrode coupling achieves an equilibrium process, $\Delta G=0$). The perturbation frequency occurs in maximum efficacy when the electrode potential is perturbed in the way that $k_r=\tau_r^{-1}$ ($\tau_r=R_{ct}C_r$), or in other words, when the resistive term is minimized whilst capacitance is maximized. Since the conductivity (inversely related to resistance) is proportional to imaginary part of capacitance (C'')[59], the peak in Bode plot corresponds to k_r. From this result, shown in Figure 4d, k_r was obtained as 35 $\pm$ 2 s^{-1}, which is in good agreement with redox tethered SAMs[59,61,62] and in the same order of magnitude of ferrocene-tagged peptide[50] about of 11 s^{-1}. At redox out potential (i.e. a potential that do not corresponds to faradaic process), the relaxation process corresponds only to SAM dipolar dielectric features that includes ion migration (i.e. $\tau=R_tC_t$)[52] whit a small parasitic contribution at the same frequency (less than 5%, inset in Figure 4d, but depend on the molecular layer characteristics it could be greater and should be evaluated carefully).

Finally, in aiming to quantify the redox activity associated with the ferrocene group incorporated to the redox-tagged peptide self-assembled monolayer, the surface coverage of the peptide SAM was determined by two different approaches. By classical voltammetry data, we estimate the surface coverage as $\Gamma=(4\pm2)x10^{-11}mol\ cm^{-2}$, and $\Gamma=(8\pm4)x10^{-11}mol\ cm^{-2}$ by capacitance spectroscopy, (calculated considering confidence interval of 95%, p-value of 0.2 for t-test average analysis), for a closely packed ferrocene modified peptide SAM considering the peptide as cylinder with a diameter of $\sim$15 Å we found$\sim$ 9.4 x 10^{-11} *mol* cm^{-2}. This theoretical estimated value is in very good agreement with those experimentally obtained from molecular coverage by ECS approach.

These values agree with theoretical data obtained assuming helical peptides, when there is a close packed and vertical arranged the value that Gatto and Venanzi make association be[43] 16.6 x $10^{-11}mol\ cm^{-2}$. Already, López-Perez and coworkers found a theoretical value of 10.0 x $10^{-11}mol\ cm^{-2}$ for studies conducted in helical peptides.[63] The peptide Ac-Ile-Ile-Lys(fc)-Ile-Ile-COOH, expressed lower compatibility, which can be explained due to the position of the ferrocene in Lys side chain, noting that in other works, the studied peptides do not have probe redox (ferrocene) in their backbones.

Comparison Electrochemical Capacitive Behaviors

It is important to know that the isoleucine-containing peptide showed a lower surface coverage compared to the alanine-containing peptide[26] and the monolayers formed by thiols[54] (Table II). This result is related to differences in the side chain volume of isoleucine and alanine. Because of the largest volume of isoleucine residues, the number of molecules per surface units that can be assembled on the gold surface is fewer than for alanine residues. On the other hand, the molecular surface coverage by thiols is larger. The alkane chain is not branched, so more molecules can be packed. These results are in accordance to the values obtained for redox capacitance. The isoleucine-containing peptide showed the lowest redox capacitance because of the low molecular surface coverage.

Table II Electrochemical Characteristics of Three Different Self-assembled Monolayers

Self-Assembled Monolayers	Molecular Surface Coverage (mol cm^{-2})	Redox Capacitance ($\mu F\ cm^{-2}$)
Ac-Cys-Ile-Ile-Lys(fc)-Ile-Ile-COOH	$(0.4 \pm 0.2)\ 10^{-10}$	105
Ac-Cys-Ala-Ala-Lys(fc)-Ala-Ala-COOH[26]	$(1.2 \pm 0.2)\ 10^{-10}$	137
Self-assembled monolayers of thiols[54]	$(3.0 \pm 1.0)\ 10^{-10}$	175

In contrast, thiol coverage showed the highest redox capacitance due to its better surface packing.

CONCLUSION

As peptides have proved to be a promising tool for the development of self-assembled monolayers we herein described a synthetic route to obtain a redox-tagged peptide able to be self-assembled over metallic surface and possessing stable and suitable electrochemical activity. The solid phase peptide synthesis allowed the sequence modification in the way to have a peptide containing an appropriate and desirable redox probe. The electrochemical performance of the redox-tagged peptide molecular layers was characterized by both cyclic voltammetry and electrochemical impedance-based capacitance spectroscopy techniques. Both techniques confirmed that the ferrocene-tagged peptide successfully provided the expected self-assembly capability of the peptide chain over gold metallic electrode with stability and electrochemical activity confirmed through the calculation of molecular coverage. Finally, the redox-tagged peptide has an additional possibility by attaching an antibody for development biosensors devices to detect directly any relevant biomarker, making use of the electrochemical capacitance signal (obtained through ECS method) intrinsically existing in redox-active monolayers.

Julia P. Piccoli acknowledges CAPES for her Ph.D. studentship. Adriano Santos acknowledges CNPq for his Ph.D. studentship (141058/2013-7).

REFERENCES

1. Tamerler, C.; Sarikaya, M. Philos Trans R Soc Lond A Math Phys Eng Sci 2009, 367, 1705–1726.
2. Dong, S.; Li, J. Bioelectrochem Bioenerg 1997, 42, 7–13.
3. Wink, T.; Van Zuilen, S.; Bult, A.; Van Bennekom, W. Analyst 1997, 122, 43R–50R.
4. Chaki, N. K.; Vijayamohanan, K. Biosens Bioelectron 2002, 17, 1–12.
5. Kulkeaw, K.; Chaicumpa, W.; Sakolvaree, Y.; Tongtawe, P.; Tapchaisri, P. Toxicon 2007, 49, 1026–1041.
6. Paulose, M.; Shankar, K.; Varghese, O. K.; Mor, G. K.; Grimes, C. A. J Phys D Appl Phys 2006, 39, 2498
7. Lee, Y. L.; Huang, B. M.; Chien, H. T. Chem Mater 2008, 20, 6903–6905.
8. Whitesides, G. M.; Kriebel, J. K.; Love, J. C. Sci Prog 2005, 88, 17–48.
9. Mandal, D.; Shirazi, A. N.; Parang, K. Org Biomol Chem 2014, 12, 3544–3561.
10. Lehn, J. M. Proc Natl Acad Sci 2002, 99, 4763–4768.
11. Ulman, A. An Introduction to Ultrathin Organic Films: From Langmuir-Blodgett to Self-Assembly; Academic Press, 2013; Chapter 3.
12. Xia, Y.; Qin, D.; Yin, Y. Curr Opin Colloid Interface Sci 2001, 6, 54–64.
13. Boozer, C.; Chen, S.; Jiang, S. Langmuir 2006, 22, 4694–4698.
14. Zhang, F.; Zhao, L.; Chen, H.; Xu, S.; Evans, D. G.; Duan, X. Angew Chem Int Ed 2008, 47, 2466–2469.
15. Nowinski, A. K.; Sun, F.; White, A. D.; Keefe, A. J.; Jiang, S. J Am Chem Soc 2012, 134, 6000–6005.
16. Newton, L.; Slater, T.; Clark, N.; Vijayaraghavan, A. J Mater Chem C 2013, 1, 376–393.
17. Lakshmanan, A.; Zhang, S.; Hauser, C. A. Trends Biotechnol 2012, 30, 155–165.
18. Yang, L.; Li, Y. Biosens Bioelectron 2005, 20, 1407–1416.
19. Zen, J. M.; Senthil Kumar, A.; Tsai, D. M. Electroanalysis 2003, 15, 1073–1087.
20. Lutz, J. F. Angew Chem Int Ed 2007, 46, 1018–1025.
21. Freire, R. S.; Pessoa, C. A.; Mello, L. D.; Kubota, L. T. J Braz Chem Soc 2003, 14, 230–243.
22. Gooding, J. J.; Mearns, F.; Yang, W.; Liu, J. Electroanalysis 2003, 15, 81–96.
23. Yang, Z.; Gonzalez-Cortes, A.; Jourquin, G.; Viré, J. C.; Kauffmann, J. M.; Delplancke, J. L. Biosens Bioelectron 1995, 10, 789–795.
24. Chaki, N. K.; Aslam, M.; Sharma, J.; Vijayamohanan, K. J Chem Sci 2001, 113, 659–670.
25. Lehr, J.; Fernandes, F. C. B.; Bueno, P. R.; Davis, J. J Anal Chem 2014, 86, 2559–2564.
26. Santos, A.; Piccoli, J. P.; Santos-Filho, N. A.; Cilli, E. M.; Bueno, P. R. Biosens Bioelectron 2015, 68, 281–287.
27. Santos, A.; Davis, J.; Bueno, P. J Anal Bioanal Tech S 2014, S7, 016. doi: 10.4172/2155-9872.S7-016.
28. Adler-Abramovich, L.; Badihi-Mossberg, M.; Gazit, E.; Rishpon, J. Small 2010, 6, 825–831.
29. Viguier, B.; Zór, K.; Kasotakis, E.; Mitraki, A.; Clausen, C. H.; Svendsen, W. E.; Castillo-León, J. ACS Appl Mater Interfaces 2011, 3, 1594–1600.
30. Plata, M. R.; Contento, A. M.; Ríos, A. Sensors 2010, 10, 2511–2576.
31. Merrifield, R. B. J Am Chem Soc 1963, 85, 2149–2154.
32. Bolduc, O. R.; Correia-Ledo, D.; Masson, J. F. Langmuir 2012, 28, 22–26.
33. Bueno, P. R.; Mizzon, G.; Davis, J. JJ Phys Chem B 2012, 116, 8822–8829.
34. Shin, D. S.; Liu, Y.; Gao, Y.; Kwa, T.; Matharu, Z.; Revzin, A. Anal Chem 2012, 85, 220–227.

35. La, M.; Zhao, X. Y.; Peng, Q. L.; Chen, C. D.; Zhao, G. Q. Int J Electrochem Sci 2015, 10, 3329–3339.
36. Adhikari, B.; Kraatz, H. B. Chem Commun 2014, 50, 5551–5553.
37. Bolduc, O. R.; Pelletier, J. N.; Masson, J. F. Anal Chem 2010, 82, 3699–3706.
38. Citartan, M.; Gopinath, S. C.; Tominaga, J.; Tan, S. C.; Tang, T. H. Biosens Bioelectron 2012, 34, 1–11.
39. Deng, D.; Shi, Y.; Feng, H.; Chen, Q.; Li, D.; Liu, L. Int J Electrochem Sci 2013, 8, 6933–6940.
40. Dijkstra, S.; Mulders, P. F.; Schalken, J. A. Clin Biochem 2014, 47, 889–896.
41. Li, H.; Huang, Y.; Zhang, B.; Yang, D.; Zhu, X.; Li, G. Theranostics 2014, 4, 701
42. Wang, N.; She, Z.; Lin, Y. C.; Martić, S.; Mann, D. J.; Kraatz, H. B. Chemistry 2015, 21, 4988–4999.
43. Gatto, E.; Venanzi, M. Polym J 2013, 45, 468–480.
44. Trasatti, S.; Petrii, O. Pure Appl Chem 1991, 63, 711–734.
45. Walczak, M. M.; Popenoe, D. D.; Deinhammer, R. S.; Lamp, B. D.; Chung, C.; Porter, M. D. Langmuir 1991, 7, 2687–2693.
46. Fontanive, G.; Berti, F. Libraries of short receptors peptides and antibodies for the recognition of small organic molecules. Ph.D. Dissertation, Università degli studi di Trieste, Trieste, TS, 2010.
47. Wain, A. J.; Do, H. N.; Mandal, H. S.; Kraatz, H. B.; Zhou, F. J Phys Chem C 2008, 112, 14513–14519.
48. Montalbetti, C. A.; Falque, V. Tetrahedron 2005, 61, 10827–10852.
49. Eckermann, A. L.; Feld, D. J.; Shaw, J. A.; Meade, T. J Coord Chem Rev 2010, 254, 1769–1802.
50. Longo, E.; Wright, K.; Caruso, M.; Gatto, E.; Palleschi, A.; Scarselli, M.; De Crescenzi, M.; Crisma, M.; Formaggio, F.; Toniolo, C.; Venanzi, M. Nanoscale 2015, 7, 15495–15506.
51. Bueno, P. R.; Benites, T. A.; Davis, J. J Sci Rep 2016, 6, 18400
52. Goes, M. S.; Rahman, H.; Ryall, J.; Davis, J. J.; Bueno, P. R. Langmuir 2012, 28, 9689–9699.
53. Bueno, P. R.; Fabregat-Santiago, F.; Davis, J. J Anal Chem 2012, 85, 411–417.
54. Fernandes, F. C.; Santos, A.; Martins, D. C.; Goes, M. S.; Bueno, P. R. Biosens Bioelectron 2014, 57, 96–102.
55. Santos, A.; Carvalho, F. C.; Roque-Barreira, M. C.; Bueno, P. R. Biosens Bioelectron 2014, 62, 102–105.
56. Wade, D.; Boman, A.; Wåhlin, B.; Drain, C. M.; Andreu, D.; Boman, H. G.; Merrifield, R. B. Proc Natl Acad Sci USA 1990, 87, 4761–4765.
57. Fernandes, F. C. B.; Góes, M. S.; Davis, J. J.; Bueno, P. R. Biosens Bioelectron 2013, 50, 437–440.
58. Bueno, P. R.; Fabregat-Santiago, F.; Davis, J. J Anal Chem 2013, 85, 411–417.
59. Bueno, P. R.; Davis, J. J Anal Chem 2014, 86, 1337–1341.
60. Bueno, P. R.; Davis, J. J Anal Chem 2014, 86, 1997–2004.
61. Bueno, P. R.; Mizzon, G.; Davis, J. J. J Phys Chem B 2012, 116, 8822–8829.
62. Bueno, P. R.; Davis, J. J. Anal Chem 2014, 86, 1977–2004.
63. López-Pérez, D. E.; Revilla-López, G.; Jacquemin, D.; Zanuy, D.; Palys, B.; Sek, S.; Alemán, C. Phys Chem Chem Phys 2012, 14, 10332–10344.